TOTEM Note
10 February 2009

Acceptance of Protons in the TOTEM RP Detectors for LHC V6.500 Early Collision Optics ($\mathbf{E = 5\,TeV}$, $\boldsymbol{\beta^* = 3\,m}$)

Hubert Niewiadomski

Abstract

This note reports about the acceptance of elastically and diffractively scattered protons in the TOTEM Roman Pot detectors, placed 147 m and 220 m away from the IP5, for the LHC early collision optics with beam energy $E = 5\,\mathrm{TeV}$ and $\beta^* = 3\,\mathrm{m}$. The results are based on thin lens proton tracking with the use of MADX and the aperture model of the machine.

The paper discusses also the behaviour of the optical functions at the Roman Pot locations as a function of the fractional proton momentum loss and reports its influence on the detection of diffractively scattered protons. The optical functions are obtained from proton tracks by means of multidimensional polynomial approximation.

1 Introduction

The TOTEM experiment [1, 2] is interested in detection of the intact protons scattered from the IP5. Such protons are measured by the near-beam telescopes, called Roman Pots (RP), placed at a distance of about 147 m and 220 m on both sides of IP5 (see [1] and [2]).

A proton produced in a diffractive interaction with the kinematic parameters[1] t, ϕ, ξ, x^*, y^*, passes a Roman Pot (RP) detector plane, placed at distance s from IP5, at a transverse position $(x(s), y(s))$ determined by the beam optics between the interaction point and the RP. The displacement $(x(s), y(s))$ is related to its transverse origin (x^*, y^*) and its momentum vector (expressed by the horizontal and vertical scattering angles Θ_x^* and Θ_y^* and by $\xi = \Delta p/p$) at the IP via the optical functions and the horizontal dispersion $D_x(s)$ of the machine:

$$\begin{aligned} x(s) &= \Delta x(s) + v_x(s) \cdot x^* + L_x(s) \cdot \Theta_x^* + \xi \cdot D_x(s) \\ y(s) &= v_y(s) \cdot y^* + L_y(s) \cdot \Theta_y^*. \end{aligned} \tag{1}$$

[1] The four momentum transfer squared is defined as $t = (E - E')^2 - (\vec{p} - \vec{p}')^2$, where the primed variables denote the quantities after the interaction. t can be also expressed [6] in terms of the scattering angle Θ, the initial momentum p, the proton mass m and the fractional momentum loss $\xi = \frac{p-p'}{p}$: $-t = -t_0 + 4p^2(1-\xi)\sin^2\frac{\Theta}{2}$ with the kinematic limit $-t_0 = 2\ p^2 + m^2\ \ \sqrt{1 + \frac{p^2(\xi^2-2\xi)}{p^2+m^2}} - 1\ \ + 2\xi p^2$.

The coefficients of Equation 1 depend upon the betatron function $\beta(s)$ and the phase advance $\Delta\mu(s)$ [3]. The functions $v(s)$ and $L(s)$ can be expressed as:

$$\begin{aligned} v(s) &= \sqrt{\frac{\beta(s)}{\beta^*}}\cos\Delta\mu(s) \\ L(s) &= \sqrt{\beta(s)\beta^*}\sin\Delta\mu(s) \\ \text{with}\quad \Delta\mu(s) &= \int_0^s \frac{1}{\beta(s')}ds'. \end{aligned} \tag{2}$$

The offset of the beam closed orbit with respect to the machine reference orbit is expressed by $\Delta x(s)$. In addition, the presence of the crossing angle at IP5 may introduce the beam tilt with respect to the reference orbit.

The Roman Pot detectors are placed at the transverse distance of $10 \times \sigma_{x,y} + 0.5\,\text{mm}$ from the beam centre, where $\sigma_{x,y}$ is the beam size at the location of the detector. The arrangement of the horizontal and vertical detectors in a single unit is presented in Figure 1.

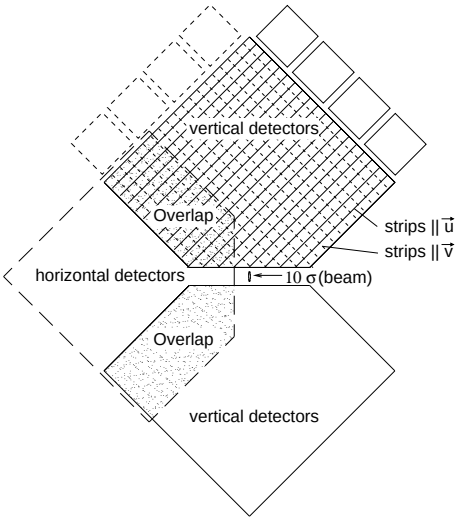

Figure 1: The overlap between the horizontal and vertical detectors.

The values of the effective lengths L_x and L_y (together with the beam size) determine the acceptance of the proton four momentum transfer $-t \approx p^2\,\Theta^{*2}$, where $p = 5\,\text{TeV}$ is the proton momentum and Θ^* is the scattering angle. Higher values of $L_{x,y}$ allow for detection of lower scattering angles and thus lower $|t|$ values. The value of the dispersion D_x determines the acceptance of $|\xi|$ for diffractively scattered protons. The magnifications v_x and v_y express the influence of primary vertex position on the proton displacement at a given RP location. In case of the analysed optics the beam size at the IP5 is small ($45.9\,\mu\text{m}$) and the magnification is not particularily important.

The discussed collision optics is characterised by the parameters given in Table 1. The optical functions, and thus the acceptances, are very similar to the ones of the target LHC collision optics with $E = 7\,\text{TeV}$ and $\beta^* = 0.55\,\text{m}$ [4]. The difference lies mainly in

the slightly lower collision energy, higher β^* and the crossing angle in IP5 which, for the studied optics, is equal to 0. Therefore, there is no beam displacement neither in IP5 nor at the insertions of the Roman Pots.

Beam energy	5 TeV
Lorentz γ	5328.9
Normalised emittance ϵ_N	3.75 μm rad
β^*	3 m
Beam size $\sigma^*_{x,y}$	45.9 μm
Beam divergence $\sigma(\Theta^*_{x,y})$	15.3 μrad
Half crossing angle $\Theta_{x,c}$	0.0 μrad
Beam offset Δx^*	0.0 μm

Table 1: Beam parameters in IP5.

The studies were carried out with the MADX [7] accelerator design programme. The optics parameters presented in Tables 1, 2 and 3 were computed with the Twiss Module, Equation (2) and standard accelerator optics formulae discussed in [3, 9], while the calculations of acceptance and chromaticity were based upon the Thin-Lens Tracking Module and the aperture database of the LHC [8]. The primary vertex and beam divergence smearing was not included in this study. Although they may only slightly affect the reported acceptance, especially beam divergence will be one of the limiting factors of proton reconstruction resolution. Since the LHC beams are characterised by similar optics in the proximity of IP5, only LHC Beam 1 was analysed.

On the basis of the protons tracked through the lattice of the LHC, the multidimensional polynomial parameterisations of the transport were computed with the method discussed in detail in [9]. The approximations obtained were used to present the dependence of the optical functions upon the proton fractional momentum loss $\xi = \Delta p/p$. All the optics related calculations were performed within the optics software package of TOTEM.

2 Acceptance in RP 147

2.1 Elastic protons

The values of the optical functions and the positions of the RPs in the RP147 station are given in Table 2. The values of the effective lengths in horizontal and vertical projection are similar and result in the acceptance for elastically scattered protons in both horizontal and vertical RPs. The lower limit of the $|t|$-acceptance is determined by the interplay of the beam size and the value of the effective length, while the upper one is defined by the machine apertures — protons scattered at larger angles are absorbed by LHC elements. The acceptance of elastically scattered protons in the RP147 station extends over the range of $0.7 < -t < 14$ GeV^2. The acceptance is much higher in case of the vertical RP (Figure 2, right) than in the horizontal one (Figure 2, left). The elastically scattered

Magnification v_x	-1.87
Magnification v_y	-2.20
Effective length L_x	19.11 m
Effective length L_y	30.15 m
Dispersion D_x	-0.082 m
Beam size σ_x	0.31 mm
Beam size σ_y	0.47 mm
Beam offset Δx	0.0 mm
Beam tilt Θ_x	0.0 μrad
RP distance from beam centre x_{RP} ($10\,\sigma_x + 0.5$ mm)	3.5 mm
RP distance from beam centre y_{RP} ($10\,\sigma_y + 0.5$ mm)	5.2 mm

Table 2: Beam and RP parameters at 147 m from IP5 for $\xi = 0.0$.

protons visible in the horizontal RP can be considered as a background for diffractive proton detection which is performed primarily by the horizontal RPs.

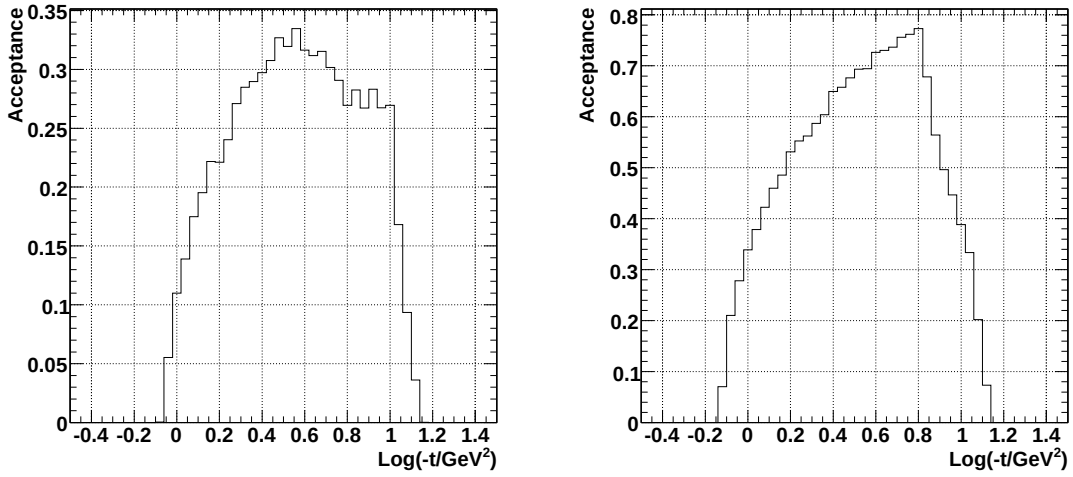

Figure 2: Acceptance of elastically scattered protons in the RP147 station. Left: Horizontal RP. Right: Vertical RP.

The acceptance of the overlapping region between the horizontal and vertical RP detectors of a given station, visible in Figure 1, is of particular interest for alignment procedures. Since in case of the analysed optics the detectors are placed only a few millimetres from the beam centre, the overlap area of the RP147 stations is characterised by acceptance exceeding 10 % for $2.2 < -t < 11$ GeV^2.

The and/or acceptance of the vertical and horizontal pots is presented in Figure 3 (left).

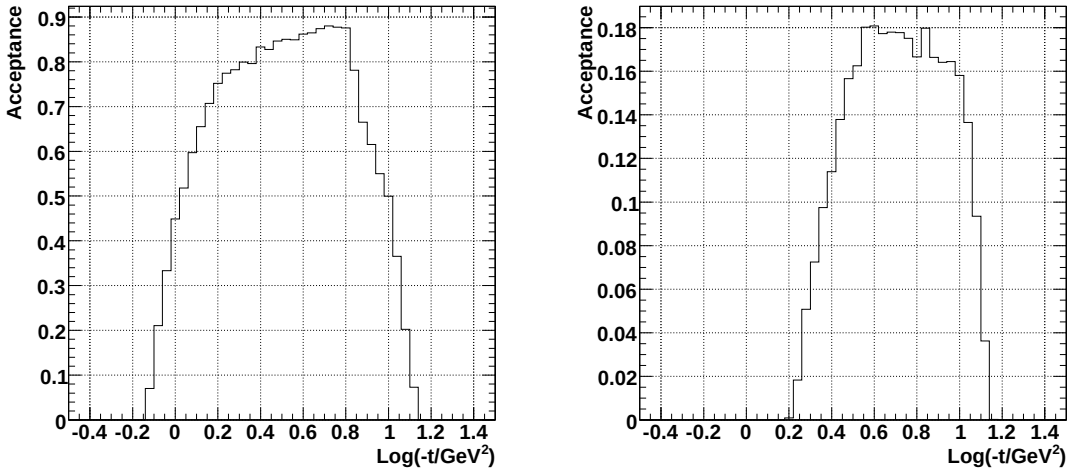

Figure 3: Acceptance of elastically scattered protons in the RP147 station. Left: The combined and/or acceptance of the horizontal and vertical RPs. Right: Acceptance of the overlap of the horizontal and vertical RPs.

2.2 Diffractive protons

The optical functions for the 5 TeV running scenario, obtained with MADX, exhibit a large dependence upon the fractional momentum loss of the proton.

The magnification values are presented in Figure 4. Although they will slightly affect the reconstruction resolution, they are not affecting the acceptance in a significant way.

The dependence of the horizontal and vertical effective lengths upon ξ is shown in Figure 5. For $\xi = 0$, L_x and L_y are 19 and 31 m, respectively. With increasing fractional

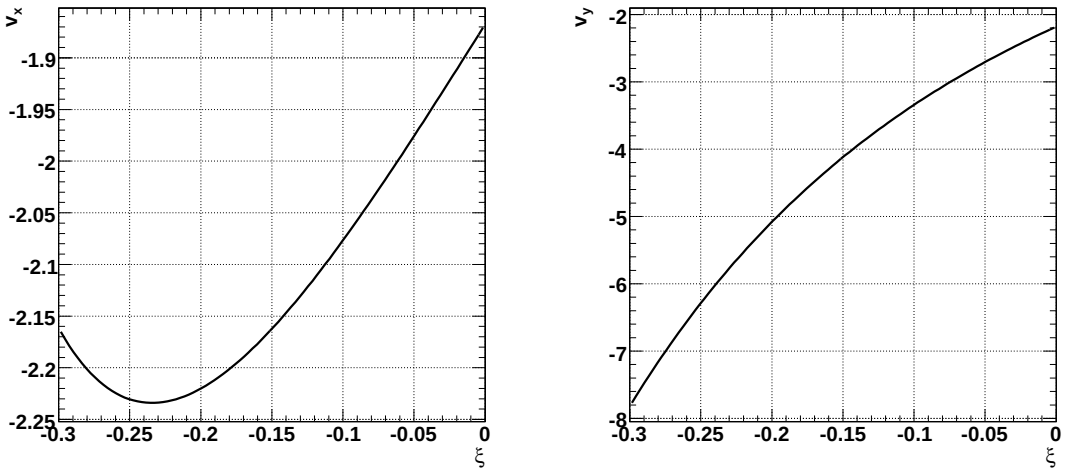

Figure 4: Magnification $v_x(\xi) = \partial x(s)/\partial x^*$ (left) and $v_y(\xi) = \partial y(s)/\partial y^*$ (right) at $s = 147$ m from IP5 as a function of the fractional proton momentum loss ξ.

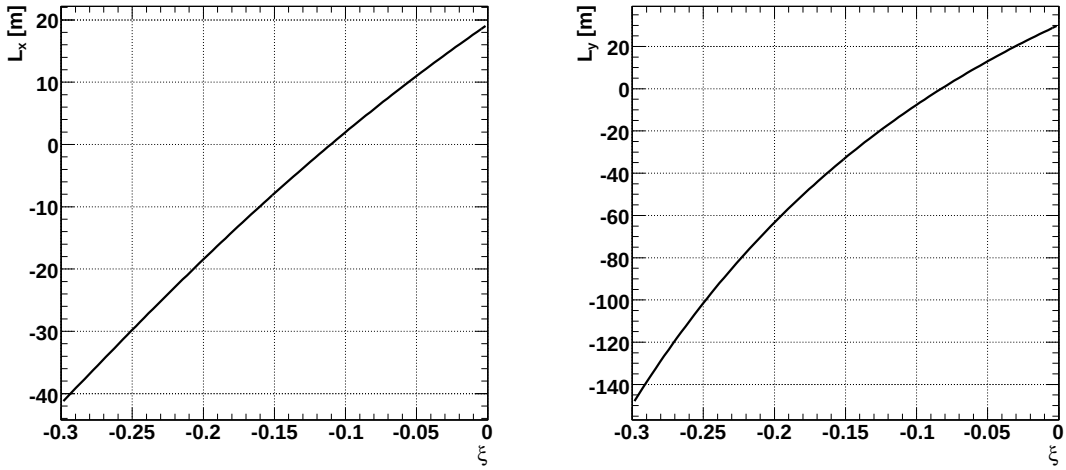

Figure 5: Effective lengths $L_x(\xi) = \partial x(s)/\partial\Theta_x^*$ (left) and $L_y(\xi) = \partial y(s)/\partial\Theta_y^*$ (right) at $s = 147\,\mathrm{m}$ from IP5 as a function of the fractional proton momentum loss ξ.

momentum loss they are reduced, reaching zero at $\xi = -0.125$ and $\xi = -0.08$, respectively. For such ξ the reconstruction of, respectively, the horizontal or vertical component of the proton scattering angle is not possible. For higher fractional momentum losses the effective lengths further decrease reaching high values with negative sign (especially L_y). This results in acceptance of the diffractively scattered protons not only in the horizontal RPs but also in the vertical ones.

The dispersion function, which is shown in Figure 6, also exhibits a ξ-dependence, which will affect the ξ-reconstruction resolution.

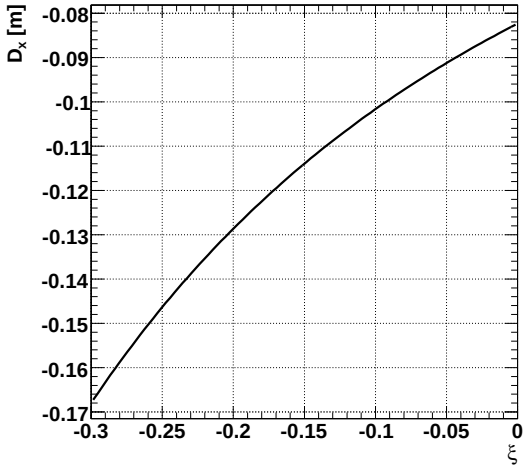

Figure 6: Dispersion $D_x(\xi) = \partial x(s)/\partial\xi$ at $s = 147\,\mathrm{m}$ from IP5 as a function of the fractional proton momentum loss ξ.

The acceptance of diffractively scattered protons in horizontal and vertical RPs is shown in Figure 7. For higher momentum losses ($-\xi > 0.04$) the protons are detected

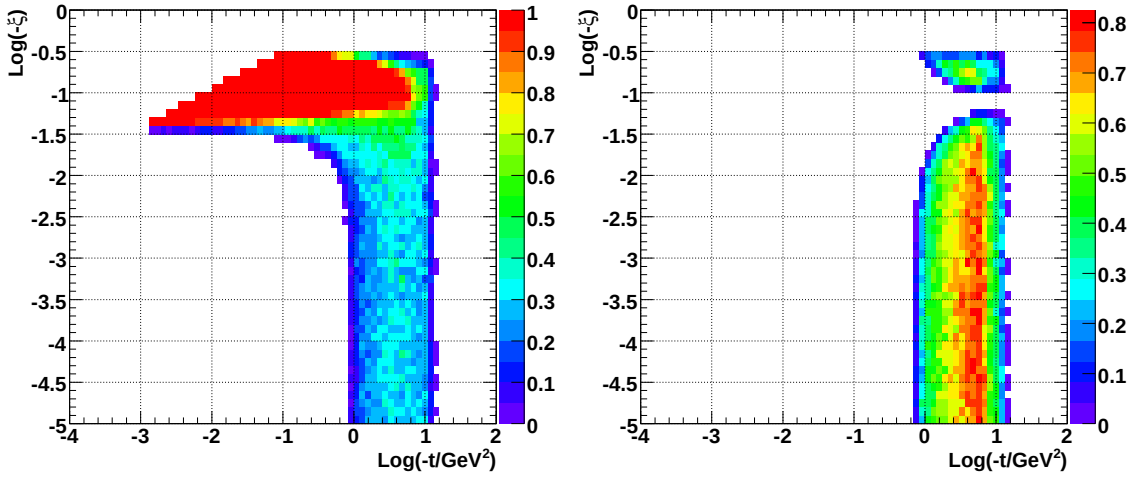

Figure 7: Acceptance in t and ξ for diffractively scattered protons in the RP147 station. Left: Horizontal RP. Right: Vertical RP.

mainly in the horizontal detectors (Figure 7, left) due to the horizontal dispersion of the machine. In this case the acceptance reaches nearly 100 %. For lower $|\xi|$-values the acceptance is due to the proton scattering angles, as in the case of the elastic scattering.

The vertical RPs also have acceptance for diffractive protons, as it is visible in Figure 7 (right). The area of acceptance for $0.13 < -\xi < 0.25$ is due to the large negative effective lengths caused by the machine chromaticity, as was presented in Figure 5. For $0.13 < -\xi < 0.06$ there is little acceptance because the effective lengths are close to 0, as was already discussed. Finally, for $-\xi < 0.06$ the acceptance in the vertical RP is again resulting from the scattering angle, as in the case of the elastic scattering.

The combined acceptance of the horizontal and vertical detectors is presented in Figure 8 (left).

The acceptance of the overlap between the horizontal and vertical RPs of the RP147 station is shown in Figure 8 (right). It extends over nearly the whole ξ-range for $2\,\mathrm{GeV}^2 < -t < 10\,\mathrm{GeV}^2$.

3 Acceptance in RP 220

3.1 Elastic protons

The optics parameters and the RP positions in the RP220 station are given in Table 3.

Since $L_x \approx 0$, the elastically scattered protons can only be detected by the vertical RPs, as can be seen in Figure 9. The acceptance extends over the range of $1\,\mathrm{GeV}^2 < -t < 13\,\mathrm{GeV}^2$ and reaches about 70 %.

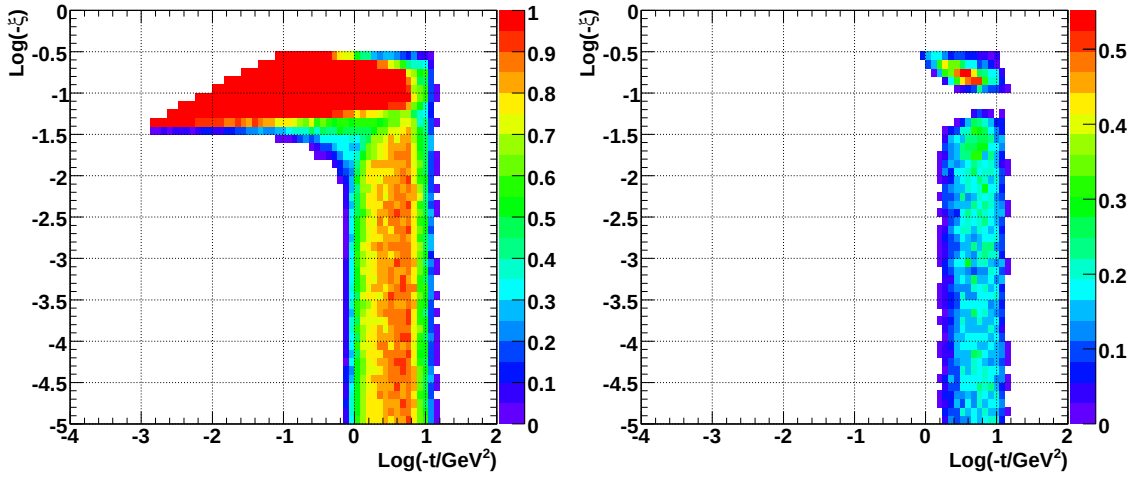

Figure 8: Acceptance in t and ξ for diffractively scattered protons in the RP147 station. Left: Total acceptance in horizontal and vertical RPs. Right: Acceptance in the overlap area of the horizontal and vertical RPs.

Magnification v_x	-3.07
Magnification v_y	-4.31
Effective length L_x	0.25 m
Effective length L_y	21.36 m
Dispersion D_x	-0.089 m
Beam size σ_x	0.14 mm
Beam size σ_y	0.38 mm
Beam offset Δx	0 mm
Beam tilt θ_x	0 μrad
RP distance from beam centre x_{RP} $(10\,\sigma_x + 0.5\,\mathrm{mm})$	1.9 mm
RP distance from beam centre y_{RP} $(10\,\sigma_y + 0.5\,\mathrm{mm})$	4.3 mm

Table 3: Values of optical functions at 219.5 m from IP5 for $\xi = 0.0$.

3.2 Diffractive protons

The optical functions at the RP220 station also exhibit the dependence upon the proton momentum loss. Figure 10 shows the evolution of the magnification as a function of ξ. Also the effective lengths decrease with increasing $|\xi|$, which is shown in Figure 11.

L_x is approximately 0 for $\xi = 0$ and becomes negative for higher fractional momentum losses. The effective length in the vertical projection is $L_y = 21\,\mathrm{m}$. For $\xi \approx -0.04$, L_y becomes zero. As it was mentioned before, when the effective length is precisely 0 the scattering angle reconstruction is impossible.

The fact that L_x and L_y reach the values of minus few tens of meters for higher fractional momentum losses allows for the detection of diffractive protons not only in the

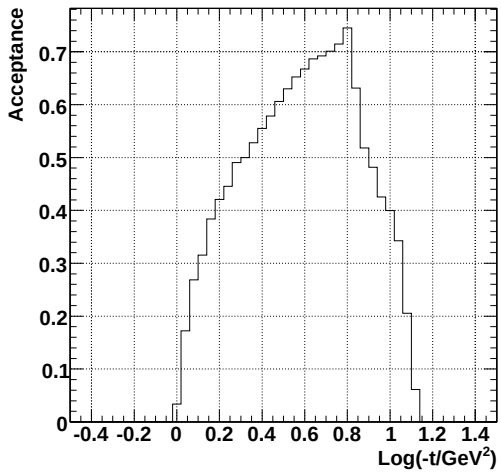

Figure 9: Acceptance of elastically scattered protons in the vertical RPs of RP220 station.

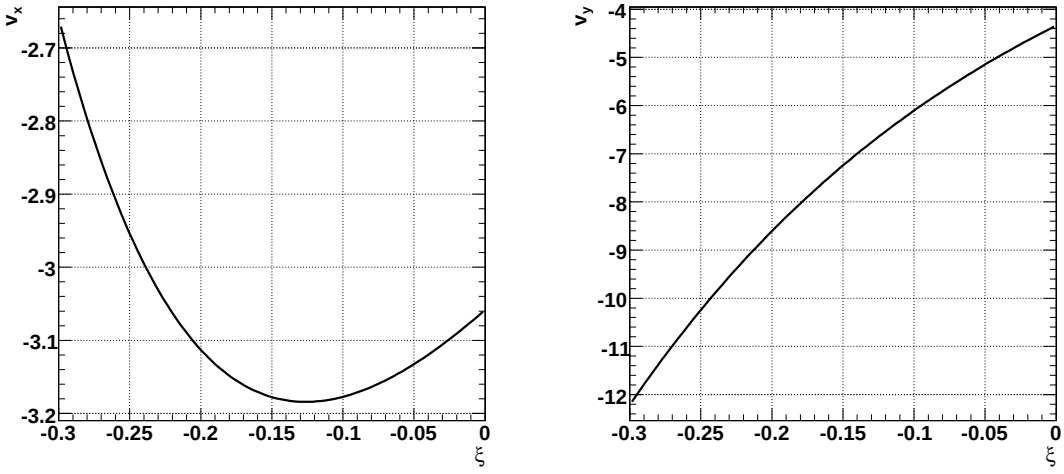

Figure 10: Magnification $v_x(\xi) = \partial x(s)/\partial x^*$ (left) and $v_y(\xi) = \partial y(s)/\partial y^*$ (right) at $s = 219.5\,\mathrm{m}$ from IP5 as a function of the fractional proton momentum loss ξ.

horizontal RPs, but also in the vertical ones, as is presented in Figure 13 (right).

The evolution of the dispersion with respect to ξ is rather limited, as can be seen in Figure 12.

The acceptance of diffractively scattered protons in the horizontal and vertical detectors of the RP220 station, for the discussed optics, is presented in Figure 13. Since L_x is low, the acceptance in horizontal RP (left plot) is only due to dispersion, which deviates protons of lower momentum in the horizontal direction. The protons are detected for $0.02 < -\xi < 0.16$, and the acceptance reaches nearly 100 %. Compared to the ξ-acceptance in the RP147 station (see Figure 7, left), the acceptance is shifted towards

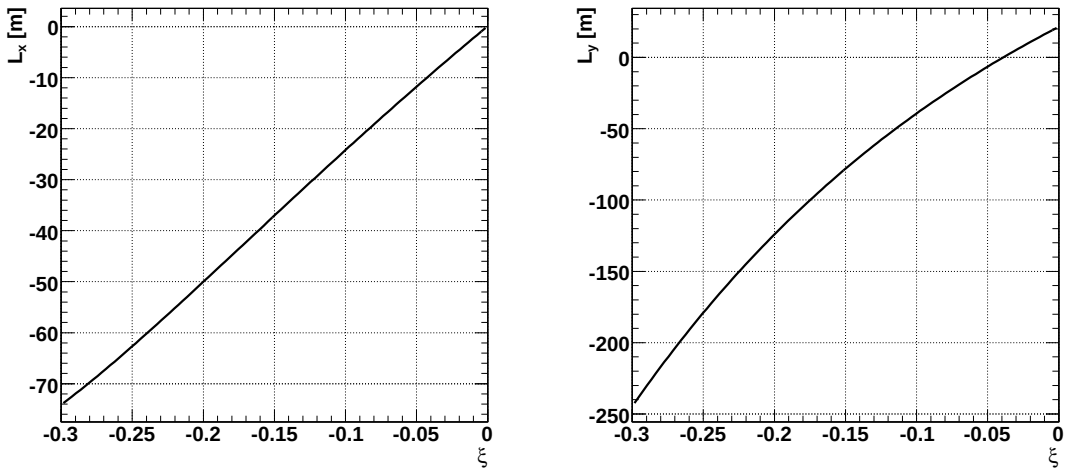

Figure 11: Effective lengths $L_x(\xi) = \partial x(s)/\partial\Theta_x^*$ (left) and $L_y(\xi) = \partial y(s)/\partial\Theta_y^*$ (right) at $s = 219.5\,\mathrm{m}$ from IP5 as a function of the fractional proton momentum loss ξ.

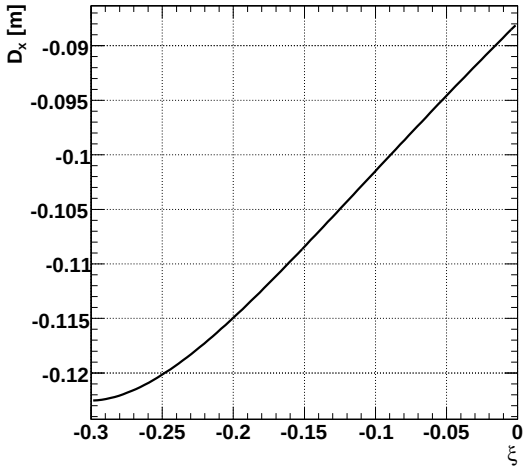

Figure 12: Dispersion $D_x(\xi) = \partial x(s)/\partial\xi$ at $s = 219.5\,\mathrm{m}$ from IP5 as a function of the fractional proton momentum loss ξ.

lower ξ-values.

The acceptance of the vertical RPs, presented in Figure 13 (right), results from high absolute values of the vertical effective length L_y. The area of acceptance in ξ and t variables is composed of two discontinuous regions separated by a gap for $0.02 < -\xi < 0.06$, when L_y changes sign and thus crosses 0.

The acceptance of the overlap area is defined by the conjunction of the left and right plots of Figure 13. As is visible in Figure 14 (right), it is limited only to higher fractional momentum losses: $-\xi > 0.01$.

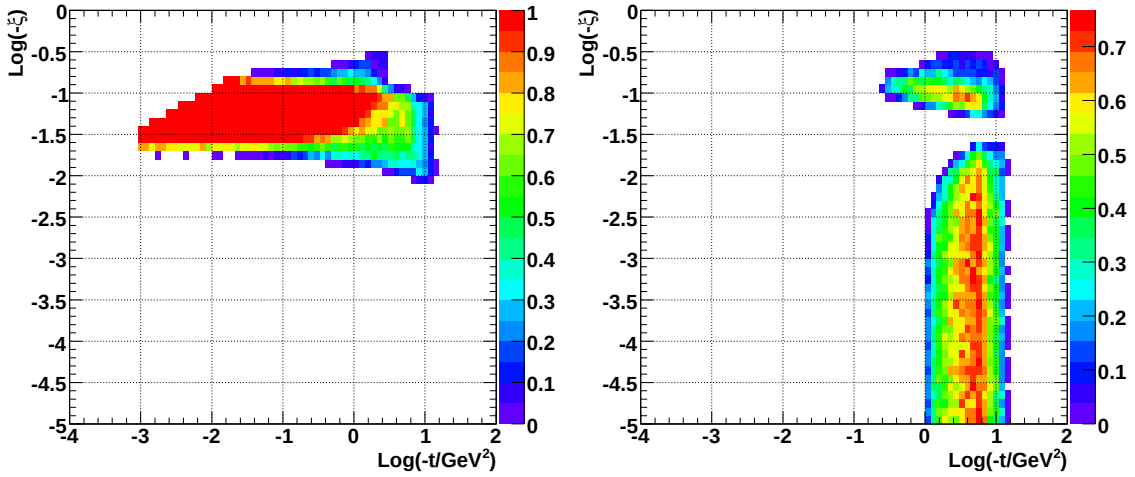

Figure 13: Acceptance in t and ξ for diffractively scattered protons in the RP220 station. Left: Horizontal RP. Right: Vertical RP.

The combined acceptance of the RP220 station is presented in Figure 14, left.

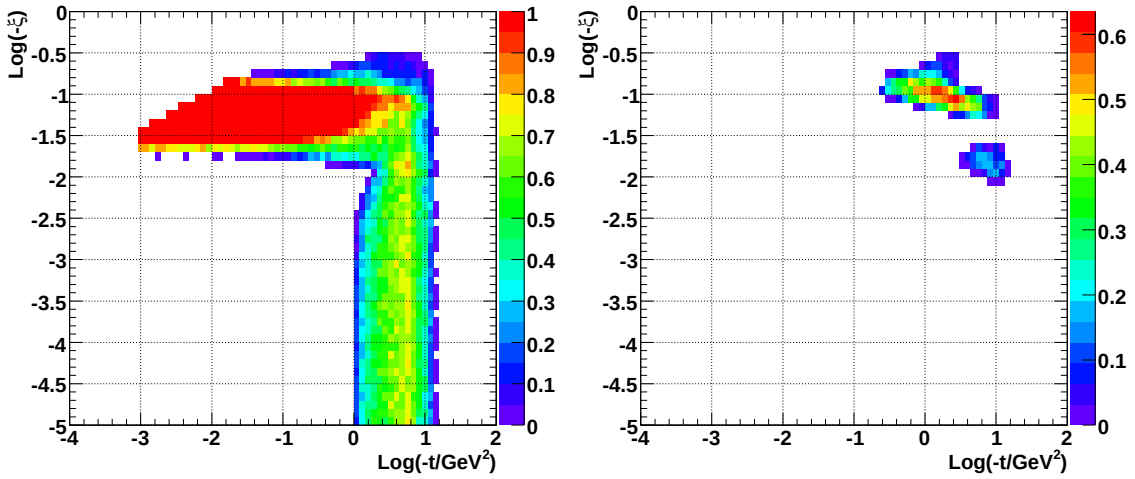

Figure 14: Acceptance in t and ξ for diffractively scattered protons in the RP220 station. Left: Combined acceptance in horizontal and vertical RPs. Right: Acceptance in the overlap area of the horizontal and vertical RPs.

References

[1] TOTEM: Technical Design Report, CERN-LHCC-2004-002; addendum CERN-LHCC-2004-020.

[2] The TOTEM Collaboration, "The TOTEM Experiment at the LHC", 2008 JINST 3 S08007, doi: 10.1088/1748-0221/3/08/S08007.

[3] E. Wilson, "An Introduction to Particle Accelerators", Oxford University Press, 2006.

[4] V. Avati, K. Oesterberg, "Acceptance calculation methods for beta*=0.5 m optics", TOTEM-NOTE 2005-002, 2005.

[5] V. Avati, K. Oesterberg, "Optical function parametrization for beta*=1540 m optics", TOTEM-NOTE 2005-001, 2005.

[6] M. Deile, "Algebraic Determination of Roman Pot Acceptance and Resolution with the $\beta^* = 1540$ m Optics", TOTEM-NOTE 2006-002.

[7] The MAD-X Home Page, http://frs.home.cern.ch/frs/Xdoc/mad-X.html.

[8] http://proj-lhc-optics-web.web.cern.ch/proj-lhc-optics-web/V6.500/.

[9] H. Niewiadomski, "Reconstruction of Protons in the TOTEM Roman Pot Detectors at the LHC", Ph. D. Thesis, University of Manchester, United Kingdom, 2008.